Negative Longitudinal Magnetoresistance from the Anomalous $N = 0$ Landau Level in Topological Materials

B. A. Assaf,[1] T. Phuphachong,[2] E. Kampert,[3] V. V. Volobuev,[4,5] P. S. Mandal,[6] J. Sánchez-Barriga,[6] O. Rader,[6] G. Bauer,[4] G. Springholz,[4] L. A. de Vaulchier,[2] and Y. Guldner[2]

[1]*Département de Physique, Ecole Normale Supérieure, PSL Research University, CNRS, 24 rue Lhomond, 75005 Paris, France*
[2]*Laboratoire Pierre Aigrain, Ecole Normale Supérieure, PSL Research University, CNRS, Université Pierre et Marie Curie, Sorbonne Universités, Université Denis Diderot, Sorbonne Cité, 24 rue Lhomond, 75005 Paris, France*
[3]*Dresden High Magnetic Field Laboratory (HLD-EMFL), Helmholtz-Zentrum Dresden-Rossendorf, 01328 Dresden, Germany*
[4]*Institut für Halbleiter und Festkörperphysik, Johannes Kepler Universität, Altenberger Straβe 69, 4040 Linz, Austria*
[5]*National Technical University "Kharkiv Polytechnic Institute", Frunze Street 21, 61002 Kharkiv, Ukraine*
[6]*Helmholtz-Zentrum Berlin für Materialien und Energie, Albert-Einstein Straβe 15, 12489 Berlin, Germany*

(Received 29 April 2017; published 8 September 2017)

Negative longitudinal magnetoresistance (NLMR) is shown to occur in topological materials in the extreme quantum limit, when a magnetic field is applied parallel to the excitation current. We perform pulsed and dc field measurements on $Pb_{1-x}Sn_xSe$ epilayers where the topological state can be chemically tuned. The NLMR is observed in the topological state, but is suppressed and becomes positive when the system becomes trivial. In a topological material, the lowest $N = 0$ conduction Landau level disperses down in energy as a function of increasing magnetic field, while the $N = 0$ valence Landau level disperses upwards. This anomalous behavior is shown to be responsible for the observed NLMR. Our work provides an explanation of the outstanding question of NLMR in topological insulators and establishes this effect as a possible hallmark of bulk conduction in topological matter.

DOI: 10.1103/PhysRevLett.119.106602

The emergence of topological insulators (TI) as novel quantum materials [1–3] has played a key role in the discovery of novel physical phenomena [4–9], such as the quantum spin Hall effect [4,10,11] and the quantum anomalous Hall effect [5,12,13]. This stems from the helical Dirac nature of surface states in 3D TIs or, that of edge states in 2D TIs. In fact, much literature (for reviews, see Refs. [14–17]) explored this question and investigated electronic transport of 2D Dirac electrons in 3D TIs. The majority of these studies were, however, impeded by the significant and dominant bulk transport that occurs in TIs. On the other hand, little attention has been given to signatures of nontrivial band topology in 3D electron transport in a TI.

Naively speaking, one can think of the bulk energy bands of a TI as being identical to those of conventional semiconductors and, thus, unlikely to generate nonconventional physical phenomena. However, one should not forget that the basis of a topological insulator lies in the inverted orbital character of these bulk energy bands [10,18]. Most interesting is the unusual behavior of the Landau levels of TIs that one can analytically extract from a general Bernevig-Hughes-Zhang Hamiltonian (appendix of Ref. [18]). In fact, it has been both theoretically [18–20] and experimentally [21–23] shown that the energy of the lowest ($N = 0$) conduction (valence) Landau level in topological insulators decreases (increases) as a function of increasing magnetic field, opposite to what usually happens in a topologically trivial system [Figs. 1(a), 1(b)]. This behavior is anomalous and leads to a field-induced closure of the energy gap in a TI [21] [Fig. 1(b)], whereas in a trivial material, the energy gap usually opens with increasing magnetic field [Fig. 1(a)]. This anomaly is a hallmark of the inverted band structure of topological materials. Its implications on magnetotransport have not yet been considered.

In the present work, we study the MR in topological insulators in the extreme quantum limit—the regime where only the lowest Landau level (LL) is occupied. We measure magnetotransport in pulsed magnetic field up to 61 T in high mobility $Pb_{1-x}Sn_xSe$ epitaxial layers. We show that, when all Lorentz contributions to the MR are suppressed by applying the magnetic field in-plane and parallel to the excitation current, a negative longitudinal MR (NLMR) emerges near the onset of the quantum limit. This NLMR is only observed in the topological regime of $Pb_{1-x}Sn_xSe$ ($x > 0.16$) and is absent in trivial samples ($x < 0.16$). We theoretically argue that this NLMR is a result of the anomalous behavior of the $N = 0$ LL that leads to a field induced closure of the energy gap as a function of the applied magnetic field, thus enhancing the carriers' Fermi velocity and reducing electrical resistivity. Our findings establish that NLMR is a hallmark of the topological insulating state, and may reconcile controversial interpretations of axial anomaly-induced NLMR in such materials.

Magnetotransport measurements are performed on [111]-oriented $Pb_{1-x}Sn_xSe$ epilayers grown on (111) BaF_2 substrates with different x. Growth by molecular beam epitaxy and characterization are described in our previous works

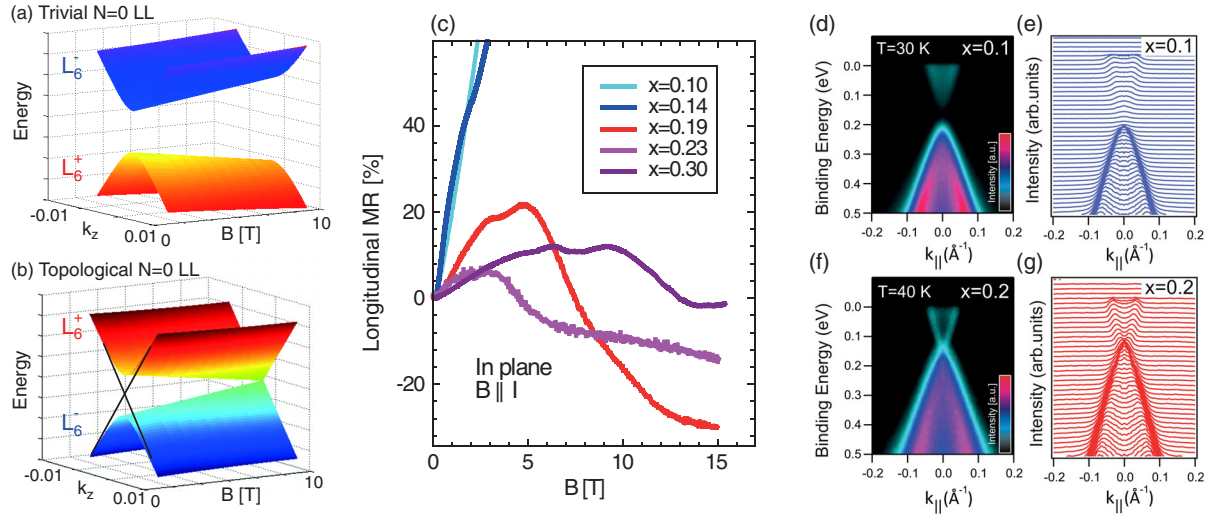

FIG. 1. Sketch of the behavior of the $N = 0$ bulk LL as a function of magnetic field for a trivial (a) and a topological (b) system. The k dispersion of the energy level in the direction of the applied field is shown (k_z). Topological surface states are shown in black in (b) at $B = 0$. The $L_6^{\pm}$ bands denote the band extrema of opposite parity occurring at the L point in $Pb_{1-x}Sn_xSe$. (c) In-plane MR measured with $B//I$ at 10 K in two trivial $Pb_{1-x}Sn_xSe$ epilayers ($x = 0.10$ and $x = 0.14$) and three topological ones ($x = 0.19$, $x = 0.23$, and $x = 0.3$) up to $B = 15$ T. ARPES dispersions and momentum distribution curves for $x = 0.1$ (d),(e) and $x = 0.2$ (f),(g) measured with 18 eV photons at 30 and 40 K, respectively.

[24–26]. A 15 T/4.2 K superconducting cryostat setup is used for in-house measurements. Further measurements are performed at 10 K up to 61 T using a 200 ms pulsed-field coil at the Dresden High Magnetic Fields Lab. Angle-resolved-photoemission (ARPES) experiments are performed with linearly polarized undulator radiation at the UE112-PGM1 beam line of the synchrotron BESSY-II in Berlin.

Figure 1(c) shows the longitudinal MR measured at 10 K, up to 15 T for five $Pb_{1-x}Sn_xSe$ samples, with the magnetic field applied in-plane parallel to the current ($I//B//$ [1–10]) (Fig. S2). For trivial samples having $x < 0.16$, [24] the MR rises fast. In nontrivial samples having $x > 0.16$ [24,27,28], although initially positive, the MR turns negative, and remains so over a wide range. The sign of the MR hence depends on the topological character of the sample.

ARPES measurements [Figs. 1(d)–1(g)] for $x = 0.10$ and $x = 0.20$ below 50 K clearly indicate the changing topological character across $x = 0.16$. A gapped state is observed in the ARPES dispersion and momentum distribution curves for $x = 0.10$ [Figs. 1(d), 1(e)] whereas for $x = 0.20$ a gapless topological Dirac surface state is clearly resolved [Figs. 1(f), 1(g)], in agreement with previous ARPES studies [27] [28]. This ties the occurrence of the NLMR to the topologically nontrivial regime in $Pb_{1-x}Sn_xSe$.

In order to confirm the robustness of the MR trend on either side of the topological phase transition, transport measurements for fields up to 61 T are performed on two selected samples with compositions close to the transition. Results are shown in Fig. 2(a). Comparing the sample

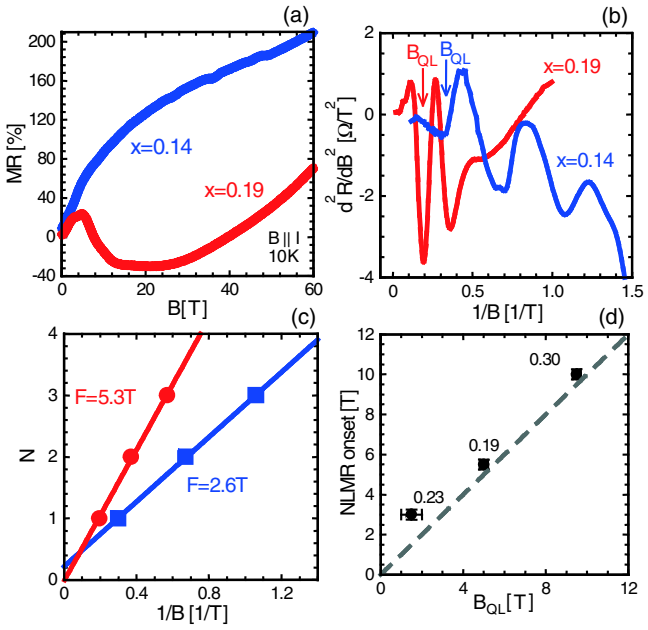

FIG. 2. (a) In-plane MR measured up to 60 T using pulsed magnetic field for $Pb_{1-x}Sn_xSe$ with $x = 0.14$ (blue) and $x = 0.19$ (red). (b) Low-field Shubnikov–de-Haas oscillations and (c) Landau index versus $1/B$ shown for both samples. Arrows mark the field at which the quantum limit is reached (B_{QL}). (d) NLMR onset extracted from Fig. 1(c) versus B_{QL} for the three topological samples considered in this work. The dashed gray line is obtained for an onset exactly equal to B_{QL}. The Sn concentration "x" corresponding to each sample is shown above the data points.

$x = 0.14$ to $x = 0.19$ confirms that the MR in the trivial regime is robustly positive up to 60 T, whereas in the topological regime, the MR is initially positive, then turns negative and reaches a plateaulike behavior at intermediate fields, then increases again at very high fields.

We correlate the appearance of the NLMR to the crossing of the $N = 1$ LL with the Fermi energy (E_f), by looking at 3D Shubnikov-de-Haas (SdH) oscillations measured in the same geometry as the MR ($I//B//$ [1–10]). Figure 2(b) shows SdH oscillations in the second derivative of the resistance for $x = 0.14$ and $x = 0.19$ at 10 K. The last oscillation minimum is observed at $B_{QL} \approx 5$ T (0.2 T^{-1}) for $x = 0.19$ and 2.8 T (0.35 T^{-1}) for $x = 0.14$; this is the onset of the extreme quantum limit [arrows in Fig. 2(b)]. The SdH frequency extracted from the plot of the Landau index N versus $1/B$ [Fig. 2(c)] comes out close to 5 T for $x = 0.19$ and 2.6 T for $x = 0.14$. For $x = 0.19$, this yields a 3D carrier density of about 6×10^{16} cm^{-3} per valley or a total of 2.4×10^{17} cm^{-3} for the four valleys of $Pb_{1-x}Sn_xSe$. This also agrees with $n_{Hall} \approx 3 \times 10^{17}$ cm^{-3} [20]. For $x = 0.14$, we find 2×10^{16} cm^{-3} per valley. The Hall data yield $p_{Hall} = 1 \times 10^{17}$ cm^{-3} for four valleys in agreement with SdH data. We also note that the SdH results nicely agree with our previous magnetooptical measurements on the same samples [24]. Even though the two samples studied here in detail have a different carrier type, the other samples examined in Fig. 1(c) rule out any link between this and the NLMR [20].

In $x = 0.19$, B_{QL} is close to the onset of the NLMR seen in Fig. 2(a). In x = 0.14, even though B_{QL} is small, no NLMR is observed up to 60 T. We consolidate the relation between the NLMR and the entrance into the quantum limit in the topological state by further investigating two additional samples ($x = 0.23$ and $x = 0.3$). Detailed SdH and magnetooptical IR spectroscopy data shown in the Supplemental Material allow us to extract B_{QL} for both [20]. The onset of the NLMR extracted from Fig. 1(c) is plotted versus B_{QL} for $x = 0.19$, $x = 0.23$, and $x = 0.3$ in Fig. 2(d). A clear correlation of the onset of NLMR with B_{QL} is observed, as indicated by the dashed line, confirming that the NLMR occurs in the quantum limit.

We next elucidate the origin of the NLMR occurring in topological materials in the quantum limit by investigating transport in this regime. We have shown that the LL in IV-IV TCIs can be well described by a massive Dirac spectrum that includes spin splitting [24,29–31], resulting from a 6-band $\mathbf{k} \cdot \mathbf{p}$ Hamiltonian [30]. If the contributions from the far bands are neglected, a 2-band $\mathbf{k} \cdot \mathbf{p}$ Hamiltonian results, the solution of which is an ideal massive Dirac model [32].

We use the 6-band Mitchell-Wallis Hamiltonian to describe the field dependence of the $N = 0$ level and its wave vector dispersion [20,30,31,33–35]:

$$E_0 = \sqrt{\left[|\Delta| \pm \left(\frac{\hbar\tilde{\omega}}{2} - \frac{\tilde{g}\mu_B B}{2}\right)\right]^2 + (\hbar v_z k_z)^2}. \quad (1)$$

The $\pm$ sign refers to the trivial and topological regime, respectively. Δ is the half-band gap, k_z is wave vector, and v_z is the Dirac velocity in the z direction ($z//B$). $\tilde{\omega} = eB/\tilde{m}$. $\tilde{m}$ and $\tilde{g}$ are the mass and effective g-factor terms resulting from interactions between the band edges and far bands located about 1 eV above and below the energy gap in the IV-VI semiconductors [30,31]. We highlight that the Mitchell-Wallis Hamiltonian is similar to the Bernevig-Hughes-Zhang (BHZ) Hamiltonian [10,18,36] that generally describes topological systems. Our treatment [Eq. (1)] can thus be generalized to any topological system exhibiting the $N = 0$ behavior shown in Fig. 1(b). The $\tilde{m}$ contribution also appears on the diagonal of the BHZ Hamiltonian as $-M_1 k^2 = [\hbar^2(k_x + k_y)^2/2\tilde{m}]$ [10,36].

For PbSe, $\tilde{g}\mu_B B \approx -\hbar\tilde{\omega}$ ($\tilde{g} \approx 2m_0/\tilde{m}$) [37]. Far-band terms vary little (<10%) with Sn content up to about $x = 0.3$, according to laser emission measurements in magnetic fields. [21] Using this result, we simplify Eq. (1) to

$$E_0 = \sqrt{(|\Delta| \pm \hbar\tilde{\omega})^2 + (\hbar v_z k_z)^2}. \quad (2)$$

In Eq. (2), the $|\Delta| \pm \hbar\tilde{\omega}$ term describes whether the energy gap closes (−) or opens (+) as a function of increasing magnetic field. At very high fields such that $|\Delta| < \hbar\tilde{\omega}$, for both the topological and trivial regime, the energy gap opens with increasing field and the $N = 0$ LL varies as given in Eq. (2) for the (+) case [20]. The field-induced gap closure in the topological regime is most likely accompanied by a topological phase transition. This effect has been treated theoretically for the QSH state in two dimensions [38] but not yet for 3D TIs and TCIs.

The LL energies are plotted versus magnetic field in Figs. 3(a) and 3(b) for $x = 0.19$ and $x = 0.14$, respectively, (and in the Supplemental Material [20] for $x = 0.23$ and $x = 0.3$). The parameters are given in the caption and in Table I. For $N = 0$, Eq. (2) is used. Notice that the $N = 0$ level is nonspin degenerate in both the topological and trivial regimes, carriers are thus fully spin polarized in the quantum limit in $Pb_{1-x}Sn_xSe$. The magnetic-field dependence of E_f is plotted in Figs. 3(a), 3(b) using

$$n_{SdH} = \frac{eB}{4\pi^2\hbar} \sum_N \int f(E_N, k_z) dk_z. \quad (3)$$

n_{SdH} is the valley carrier density, $f(E_N, k_z)$ is the Fermi-Dirac function, E_N is the LL energy. From Eq. (3), we also get $k_z(B)$ in the quantum limit:

$$k_z(B) = \frac{2\pi^2\hbar n_{SdH}}{eB}, \quad (4)$$

The magnetoconductivity for a 3D electron gas in the quantum limit, in the presence of pointlike impurities, has recently been treated by Goswami *et al.* [39] Although Ref. [39] also treated the problem of scattering by

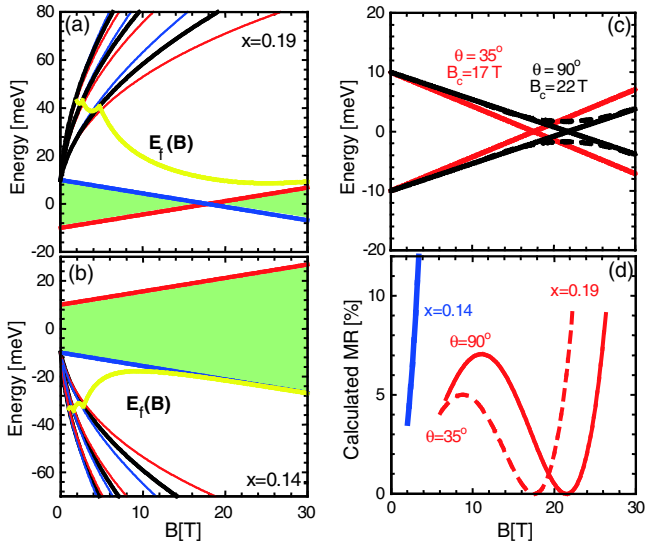

FIG. 3. Massive Dirac LL (black) and spin-split LLs (red and blue) of $Pb_{1-x}Sn_xSe$ versus magnetic field for $x = 0.19$ (a) and $x = 0.14$ (b). The energy gap is $2\Delta = 20$ meV and $v_z = 4.8 \times 10^5$ m/s for $x = 0.19$ and 5.0×10^5 m/s for $x = 0.14$.$\tilde{m} = 0.20m_0$ is used for both samples [24]. E_f versus magnetic field is shown in yellow. The energy gap is shaded in green. (c) $N = 0$ LLs for the 35° and 90° valleys computed using the parameters in Table I. (d) MR calculated using Eq. (6) for parameters shown in Table I, for $x = 0.14$ and $x = 0.19$ above the quantum limit.

long-range ionized impurities, we neglect their impact in $Pb_{1-x}Sn_xSe$ because of its very large dielectric constant (>280) [40,41]. In IV-VI systems, the scattering rate from ionized impurities is thus expected to be at least two orders of magnitude smaller than that of narrow-gap III-V or II-VI materials [39,42]. It is also well known that in $Pb_{1-x}Sn_xSe$, doping is essentially caused by atomic vacancies that can be treated as pointlike defects. From Ref. [39] we get

$$\sigma(B) = \frac{e^2\hbar}{2\pi n_i U_0} v_f^2(B). \tag{5}$$

n_i is the impurity density, U_0 is the impurity potential, and $v_f(B)$ is the Fermi velocity as a function of magnetic field. Using Eqs. (2) and (4), we obtain [39]

$$v_f(B) = \frac{\alpha v_z^2}{\sqrt{(|\Delta| \pm \frac{\hbar eB}{\tilde{m}})^2 e^2B^2 + \alpha^2 v_z^2}}, \tag{6}$$

$\alpha = 2\pi^2\hbar^2 n_{\mathrm{SdH}}$. By plugging Eq. (6) into Eq. (5), we get the MR and its derivative in the quantum limit:

$$MR = \frac{\rho(B)}{\rho(0)} - 1 = \frac{\sigma(0)}{\sigma(B)} - 1 = \left(|\Delta| \pm \frac{\hbar eB}{\tilde{m}}\right)^2 \frac{e^2B^2}{\alpha^2 v_z^2}. \tag{7}$$

$$\frac{dMR}{dB} = 2\frac{e^2B}{\alpha^2 v_z^2}\left(|\Delta| \pm \frac{\hbar eB}{\tilde{m}}\right)\left(|\Delta| \pm 2\frac{\hbar eB}{\tilde{m}}\right). \tag{8}$$

For $\Delta\tilde{m}/2\hbar e < B < \Delta\tilde{m}/\hbar e$ the derivative becomes negative in the topological regime and resistance decreases as a function of magnetic field, yielding a NLMR.

Qualitatively, this effect can be understood as follows. In the topological regime, as the gap closes, the carriers' band-edge effective mass gets smaller, and v_f gets larger. The opposite occurs when the energy gap opens [Figs. 1(a), 1(b)]. When only point-like defects are considered in the material, v_f determines the behavior of the conductivity. Therefore, a magnetic-field-induced gap closure causes a decrease in the resistance, whereas a gap opening causes an increase in resistance.

In order to plot the MR versus B using Eq. (7), a knowledge of Δ, v_z, and $\tilde{m}$ is required. The valley degeneracy and anisotropy of IV-VI materials also need to be accounted for. When $B//$ [1–10], the Fermi surface consists of two ellipsoidal valleys having their major axis tilted by $\theta = 90°$, and two others tilted by $\theta = 35°$ with respect to B (Fig. S2) [20,21]. Δ and $v_z(\theta)$ can be obtained from previous magneto-optical measurements [24]. Based on previous measurements of $\tilde{m}$, we can determine $\tilde{m}(\theta)$ [21,24]. The parameters for the angles of interest are shown in Table I.

We now compute the variation of the $N = 0$ conduction and valence LL as a function of magnetic field for both valleys for $x = 0.19$ [Fig. 3(c)], and calculate the MR using Eq. (7) for $x = 0.14$ and $x = 0.19$. In the trivial case for $x = 0.14$, the MR is positive [Fig. 3(d)], in agreement with the predictions of Goswami *et al.* for point defects [39] and with our data [Fig. 2(a)]. In the topological regime for $x = 0.19$, the model yields a negative MR when $\Delta\tilde{m}/2\hbar e < B < \Delta\tilde{m}/\hbar e$ for each valley, [Fig. 3(d)]. We get a NLMR between 11 and 22 T for the 90° valley and between 8.5 and 17 T for the 35° valley. Two MR minima are thus expected at 22 and 17 T. Experimentally, we observe a wide MR minimum at around $B_c = 20$ T [Fig. 2(a)]. The model thus agrees quantitatively with both the sign of the MR and

TABLE I. Parameters used to compute the MR shown in Fig. 3(d). The carrier density is determined from SdH measurements shown in Fig. 2. $B_c = \Delta\tilde{m}/\hbar e$ is the field at which the $N = 0$ LLs cross.

$Pb_{1-x}Sn_xSe$	n_{SdH} [per valley]	$\lvert\Delta\rvert$ [meV]	v_z [10^5 m/s] (35°, 90°)	$\tilde{m}/m_0$ (35°,90°)	B_c [T] (35°,90°)
$x = 0.14$	2×10^{16} cm^{-3}	10	5.0, 4.8	0.20 ± 0.02, 0.25 ± 0.03	N/A
$x = 0.19$	6×10^{16} cm^{-3}	10	4.8, 4.6	0.20 ± 0.02, 0.25 ± 0.03	17 ± 0, 22 ± 3

position of the MR minimum. The broadening of the miniumum can be due to the coexistence of the two minima resulting from valley degeneracy [20] and an anticrossing of $N = 0$ LL [dashed line in Fig. 3(c)] near B_c [43].

The experimental onset of the NLMR is 5 T. The model predicts an onset of about 8.5 T. The onset calculated in the model is, however, nonuniversal and strongly depends on carrier population of different valleys [44]. For simplicity, a constant carrier population of valleys is assumed, leading to Eq. (4). This is not always the case in IV-VI TCIs thin films grown on BaF_2 since the $N = 0$ LL disperse differently for different valleys and since a slight energy offset between different valleys may occur at low temperatures due to the mismatch of the expansion coefficients of the epilayers and the substrate. This causes a depopulation of one type of valleys and a repopulation of the other [44]. The most populated valley then dictates the behavior in the quantum limit; however, the carrier density in this valley will no longer be constant, resulting in a violation of Eq. (4). The onset of the NLMR will no longer be governed by the condition $\Delta\tilde{m}/2\hbar e = B$ as inferred from Eq. (7) and will only be governed by the system entering the quantum limit.

Finally, the magnitude of the simulated MR is smaller than what is observed experimentally due to the rescaling of the MR by $R(B = 0)$, assumed to be given by Eq. (5) at $B = 0$. Nevertheless, the shape of the NLMR, and its minimum agree very well with our model, without the use of any fit parameters. Most importantly, the model elucidates that the NLMR is observed in topologically nontrivial samples, and absent in trivial ones, as solely determined by the behavior of the $N = 0$ LLs. A similar effect may occur in Dirac and Weyl semimetals when Zeeman splitting shifts the $N = 0$ level in energy at high magnetic field [39,45]. In this situation, a NLMR may be observed even if the Fermi energy is located far away from the Weyl nodes, and the chirality is not well defined [46].

In conclusion, we have shown that NLMR results from the anomalous behavior of the lowest bulk LL of topological materials (Fig. 1). This MR and its anisotropy [20] are not qualitatively different from what is observed in Dirac and Weyl semimetals, as it only appears for B parallel to I [47–50]. However, its origin is fundamentally different and is not related to the chiral anomaly. It is a result of the topologically nontrivial nature of bulk bands, the anomalous behavior of the $N = 0$ Landau level and is a direct consequence of the inverted band structure of topological materials. Our results establish that NLMR is a hallmark of the topological insulating state, and can reconcile controversial interpretations of axial anomalouslike [51,52] NLMR in candidate topological insulators such as, $ZrTe_5$ [23,53], and possibly $Pb_{0.75}Sn_{0.25}Te$ under pressure [54]. It may even be extended to the quasiclassical regime to explain the occurence of NLMR in Bi_2Se_3 [55].

We acknowledge A. Ernst, O. Pankratov, S. Tchoumakov, and M. Goerbig for useful comments. We also thank G. Bastard for several fruitful discussions. This work is supported by Agence Nationale de la Recherche LabEx grant ENS-ICFP (ANR-10-LABX-0010/ANR-10-IDEX-0001-02 PSL) and by the Austrian Science Fund, Project SFB F2504-N17 IRON. T. P. acknowledges support from the Mahidol Wittayanusorn Scholarship and the Franco-Thai Scholarship. We also acknowledge the support of the HLD-HZDR, member of the European Magnetic Field Laboratory (EMFL).

[1] M. Z. Hasan and C. L. Kane, Rev. Mod. Phys. **82**, 3045 (2010).
[2] X.-L. Qi and S.-C. Zhang, Rev. Mod. Phys. **83**, 1057 (2011).
[3] C. L. Kane and E. J. Mele, Phys. Rev. Lett. **95**, 226801 (2005).
[4] M. Konig, S. Wiedmann, C. Brune, A. Roth, H. Buhmann, L. W. Molenkamp, X.-L. Qi, and S.-C. Zhang, Science **318**, 766 (2007).
[5] C.-Z. Chang, J. Zhang, X. Feng, J. Shen, Z. Zhang, M. Guo, K. Li, Y. Ou, P. Wei, L.-L. Wang, Z.-Q. Ji, Y. Feng, S. Ji, X. Chen, J. Jia, X. Dai, Z. Fang, S.-C. Zhang, K. He, Y. Wang *et al.*, Science **340**, 167 (2013).
[6] E. Bocquillon, R. S. Deacon, J. Wiedenmann, P. Leubner, T. M. Klapwijk, C. Brüne, K. Ishibashi, H. Buhmann, and L. W. Molenkamp, Nat. Nanotechnol. **12**, 137 (2016).
[7] P. Wei, F. Katmis, B. A. Assaf, H. Steinberg, P. Jarillo-Herrero, D. Heiman, and J. S. Moodera, Phys. Rev. Lett. **110**, 186807 (2013).
[8] A. R. Mellnik, J. S. Lee, A. Richardella, J. L. Grab, P. J. Mintun, M. H. Fischer, a. Vaezi, a. Manchon, E.-a. Kim, N. Samarth, and D. C. Ralph, Nature (London) **511**, 449 (2014).
[9] B. A. Assaf, F. Katmis, P. Wei, C.-Z. Chang, B. Satpati, J. S. Moodera, and D. Heiman, Phys. Rev. B **91**, 195310 (2015).
[10] B. A. Bernevig, T. L. Hughes, and S.-C. Zhang, Science **314**, 1757 (2006).
[11] I. Knez, R.-R. Du, and G. Sullivan, Phys. Rev. Lett. **107**, 136603 (2011).
[12] R. Yu, W. Zhang, H.-J. Zhang, S.-C. Zhang, X. Dai, and Z. Fang, Science **329**, 61 (2010).
[13] C.-Z. Chang, W. Zhao, D. Y. Kim, H. Zhang, B. A. Assaf, D. Heiman, S.-C. Zhang, C. Liu, M. H. W. Chan, and J. S. Moodera, Nat. Mater. **14**, 473 (2015).
[14] Y. Ando, J. Phys. Soc. Jpn. **82**, 102001 (2013).
[15] M. Veldhorst, M. Snelder, M. Hoek, C. G. Molenaar, D. P. Leusink, A. A. Golubov, H. Hilgenkamp, and A. Brinkman, Phys. Status Solidi—Rapid Res. Lett. **7**, 26 (2013).
[16] D. Culcer, Phys. E Low-Dimensional Syst. Nanostructures **44**, 860 (2012).
[17] C.-Z. Chang, P. Wei, and J. S. Moodera, MRS Bull. **39**, 867 (2014).
[18] B. A. Bernevig and T. L. Hughes, *Topological Insulator and Topological Superconductors* (Princeton University Press, Princeton, NJ, 2013).
[19] M. Orlita, B. A. Piot, G. Martinez, N. K. S. Kumar, C. Faugeras, M. Potemski, C. Michel, E. M. Hankiewicz, T. Brauner, Č. Drašar, S. Schreyeck, S. Grauer, K. Brunner,

C. Gould, C. Brüne, and L. W. Molenkamp, Phys. Rev. Lett. **114**, 186401 (2015).
[20] See Supplemental Material at http://link.aps.org/supplemental/10.1103/PhysRevLett.119.106602 for $N = 0$ Landau level from the Mitchell and Wallis Hamiltonian, Zeeman splitting and the g-factor, the far-band mass anisotropy, Hall effect results, Quantum oscillations in $x = 0.23$ and $x = 0.3$ and the MR anisotropy.
[21] A. Calawa, J. Dimmock, T. Harman, and I. Melngailis, Phys. Rev. Lett. **23**, 7 (1969).
[22] M. Schultz, U. Merkt, A. Sonntag, U. Rossler, R. Winkler, T. Colin, P. Helgesen, T. Skauli, and S. Lovold, Phys. Rev. B **57**, 14772 (1998).
[23] Z.-G. Chen, R. Y. Chen, R. D. Zhong, J. Schneeloch, C. Zhang, Y. Huang, F. Qu, R. Yu, Q. Li, G. D. Gu, and N. L. Wang, Proc. Natl. Acad. Sci. U.S.A. **114**, 816 (2017).
[24] B. A. Assaf, T. Phuphachong, V. V Volobuev, G. Bauer, G. Springholz, L.-A. de Vaulchier, and Y. Guldner, npj Quantum Mater. **2**, 26 (2017).
[25] G. Springholz and G. Bauer, in *Landolt-Bornstein*, edited by K. Klingshern (Springer Verlag, Berlin, 2013), p. 415.
[26] G. Springholz, in *Molecular Beam Epitaxy*, edited by M. Henini (Elsevier, 2013), p. 263.
[27] B. M. Wojek, P. Dziawa, B. J. Kowalski, and A. Szczerbakow, A. M. Black-Schaffer, M. H. Berntsen, T. Balasubramanian, T. Story, and O. Tjernberg, Phys. Rev. B **90**, 161202 (2014).
[28] P. Dziawa, B. J. Kowalski, K. Dybko, R. Buczko, a. Szczerbakow, M. Szot, E. Łusakowska, T. Balasubramanian, B. M. Wojek, M. H. Berntsen, O. Tjernberg, and T. Story, Nat. Mater. **11**, 1023 (2012).
[29] T. Phuphachong, B. Assaf, V. Volobuev, G. Bauer, G. Springholz, L.-A. de Vaulchier, and Y. Guldner, Crystals **7**, 29 (2017).
[30] D. L. Mitchell and R. F. Wallis, Phys. Rev. **151**, 581 (1966).
[31] G. Bauer, in *Narrow-Gap Semiconductors. Physics and Applications: Proceedings of the International Summer School*, edited by W. Zawadzki (Springer Berlin Heidelberg, 1980), p. 427.
[32] B. A. Assaf, T. Phuphachong, V. V. Volobuev, A. Inhofer, G. Bauer, G. Springholz, L. A. de Vaulchier, and Y. Guldner, Sci. Rep. **6**, 20323 (2016).
[33] H. Burkhard, G. Bauer, and W. Zawadzki, Phys. Rev. B **19**, 5149 (1979).
[34] J. Dimmock, in *Proceedings of the International Conf. Phys. Semimetals Narrow Gap Semicond. 1969*, edited by D. L. Cart and R. T. Bate (Pergamon, New York, 1971), p. 319.
[35] J. Melngailis, T. C. Harman, and W. C. Kernan, Phys. Rev. B **5**, 2250 (1972).
[36] C. X. Liu, X. L. Qi, H. J. Zhang, X. Dai, Z. Fang, and S. C. Zhang, Phys. Rev. B **82**, 045122 (2010).
[37] H. Pascher, G. Bauer, and R. Grisar, Phys. Rev. B **38**, 3383 (1988).
[38] Y. Yang, Z. Xu, L. Sheng, B. Wang, D. Y. Xing, and D. N. Sheng, Phys. Rev. Lett. **107**, 066602 (2011).
[39] P. Goswami, J. H. Pixley, and S. Das Sarma, Phys. Rev. B **92**, 075205 (2015).
[40] H. Preier, Applied Physics **20**, 189 (1979).
[41] E. Burstein, S. Perkowitz, and M. H. Brodsky, Le J. Phys. Colloq. **29**, C4-78 (1968).
[42] G. Bastard, *Wave Mechanics Applied to Semiconductor Heterostructures* (Les éditions de physique, Les Ulis, France, 1996).
[43] G. A. Baraff, Phys. Rev. **137**, A842 (1965).
[44] J. Oswald, P. Pichler, B. B. Goldberg, and G. Bauer, Phys. Rev. B **49**, 17029 (1994).
[45] R. Y. Chen, Z. G. Chen, X.-Y. Song, J. A. Schneeloch, G. D. Gu, F. Wang, and N. L. Wang, Phys. Rev. Lett. **115**, 176404 (2015).
[46] F. Arnold, C. Shekhar, S.-C. Wu, Y. Sun, R. D. dos Reis, N. Kumar, M. Naumann,M. O. Ajeesh, M. Schmidt, A. G. Grushin, J. H. Bardarson, M. Baenitz,D. Sokolov, H. Borrmann, M. Nicklas, C. Felser, E. Hassinger, and B. Yan, Nat. Commun. **7**, 11615 (2016).
[47] J. Xiong, S. K. Kushwaha, T. Liang, J. W. Krizan, M. Hirschberger, W. Wang, R. J. Cava, and N. P. Ong, Science **350**, 413 (2015).
[48] Q. Li, D. E. Kharzeev, C. Zhang, Y. Huang, I. Pletikosić, A. V. Fedorov, R. D. Zhong, J. A. Schneeloch, G. D. Gu, and T. Valla, Nat. Phys. **12**, 550 (2016).
[49] X. Huang, L. Zhao, Y. Long, P. Wang, D. Chen, Z. Yang, H. Liang, M. Xue, H. Weng, Z. Fang, X. Dai, and G. Chen, Phys. Rev. X **5**, 031023 (2015).
[50] H.-J. Kim, K.-S. Kim, J.-F. Wang, M. Sasaki, N. Satoh, A. Ohnishi, M. Kitaura, M. Yang, and L. Li, Phys. Rev. Lett. **111**, 246603 (2013).
[51] D. T. Son and B. Z. Spivak, Phys. Rev. B **88**, 104412 (2013).
[52] H. B. Nielsen and M. Ninomiya, Phys. Lett. B **130**, 389 (1983).
[53] G. Manzoni, L. Gragnaniello, G. Autès, T. Kuhn, A. Sterzi, F. Cilento, M. Zacchigna, V. Enenkel, I. Vobornik, L. Barba, F. Bisti, P. Bugnon, A. Magrez, V. N. Strocov, H. Berger, O. V. Yazyev, M. Fonin, F. Parmigiani, and A. Crepaldi, Phys. Rev. Lett. **117**, 237601 (2016).
[54] T. Liang, S. Kushwaha, J. Kim, Q. Gibson, J. Lin, N. Kioussis, R. J. Cava, and N. P. Ong, Sci. Adv. **3**, e1602510 (2017).
[55] S. Wiedmann, A. Jost, B. Fauqué, J. van Dijk, M. J. Meijer, T. Khouri, S. Pezzini, S. Grauer, S. Schreyeck, C. Brüne, H. Buhmann, L. W. Molenkamp, and N. E. Hussey, Phys. Rev. B **94**, 081302 (2016).